Process optimization for polishing large aspheric mirrors

James H. Burge*, Dae Wook Kim, and Hubert M. Martin

College of Optical Sciences and Steward Observatory Mirror Lab
University of Arizona
Tucson, AZ USA 85721

ABSTRACT

Large telescope mirrors have stringent requirements for surface irregularity on all spatial scales. Large scale errors, typically represented with Zernike polynomials, are relatively easy to control. Errors with smaller spatial scale can be more difficult because the specifications are tighter. Small scale errors are controlled with a combination of natural smoothing from large tools and directed figuring with precisely controlled small tools. The optimization of the complete process builds on the quantitative understanding of natural smoothing, convergence of small tool polishing, and confidence in the surface measurements. This paper provides parametric models for smoothing and directed figuring that can be used to optimize the manufacturing process.

Keywords: Optical fabrication, large optics, computer-controlled polishing, astronomical optics

1. INTRODUCTION

Large mirrors for astronomical telescopes have stringent requirements for surface irregularity on all spatial scales. The largest scale irregularity, typically represented with the lowest 20 or so Zernike polynomials, are controlled with a combination of polishing and active optics. Since these features are larger than the typical polishing tools, they are addressed directly by adjusting the polishing strokes to provide more dwell or more pressure over the high regions. The limitation for these modes typically comes from measurement uncertainties.

Mid-spatial frequency errors, with spatial frequency of 5 to 100 cycles across the mirror are more challenging for two reasons:
- the specifications are tighter for these errors
- available processes have limited efficiency for correcting these errors.

These errors are controlled by a combination of natural smoothing, which is the natural tendency of errors smaller than the lap size to be smoothed out, and directed figuring with smaller tools. The efficiency of both of these mechanisms tends to be slow for large aspheric mirrors. The natural smoothing relies on the size of the lap and the quality of the fit between the lap and the aspheric surface. The directed figuring of small scale errors requires small tools, which require very long run times for large mirrors. Also, the convergence of this process depends critically on the accuracy of the optical metrology. Control of surface irregularity with high-spatial-frequency, spanning the range up to 1000 cycles/m, has similar difficulty. But the control of the smallest scale errors comes primarily from the natural smoothing built into the process.

This paper provides a quantitative analysis of the relative performance and efficiency for directed figuring and natural smoothing for all spatial scales. The development of a parametric model for natural smoothing is provided in Section 2, followed by a similar treatment for directed figuring in Section 3. These effects are balanced and optimized in Section 4.

*jburge@optics.arizona.edu

2. NATURAL SMOOTHING

Optical figuring relies on the natural smoothing that occurs for lapping operations. When the lap runs over the surface, high features such as bumps see increased pressure and tend to be worn down. Low features, such as holes, see lower pressure which decreases the removal relative to the surrounding areas. This natural tendency creates surfaces that are smooth over spatial scales small compared to the lap.

Since natural smoothing relies on the stiffness of the polishing tools and the intimate contact between the lap and the workpiece, considerable effort goes in to making tools that are stiff enough to provide natural smoothing, yet maintain some compliance to fit aspheric surfaces.[1,2] Improved performance can be achieved for polishing steep aspherics using a stressed lap that deforms the shape of the lap under computer control such that it conforms to the aspheric surface.[3,4]

We quantify the natural smoothing using a dimensionless smoothing factor SF that relates the reduction of surface irregularity to the bulk DC removal from the polishing. The surface irregularity before a polishing run is denoted as ε_{ini}. After a polishing run that creates average removal of Δz, the irregularity is reduced to ε', as shown in Figure 1.

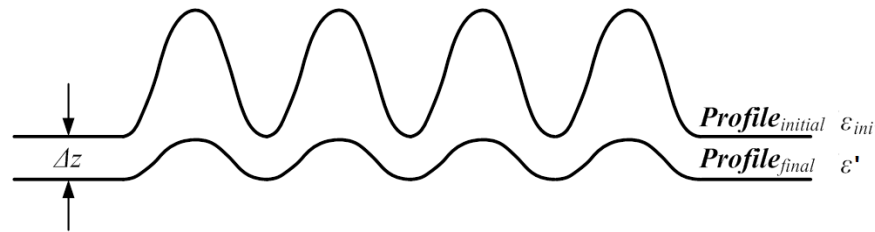**Figure 1.** Surface profiles before and after a polishing run show bulk removal Δz and smoothing that reduces the irregularity from ε_{ini} to ε'

The smoothing factor SF is defined as

$$SF = \frac{d(smooth)}{d(remove)} = \frac{\varepsilon_{ini} - \varepsilon'}{\Delta z}$$

Eq. 1

The smoothing performance of different types of tools was measured directly by creating surface irregularities and measuring the change due to smoothing as the part is polished. The smoothing for classical pitch tools and for rigid conformal polishing tools was measured over a range of surface irregularity.[5] The evolution of the surface ripples for both tools is shown below in Figure 2.
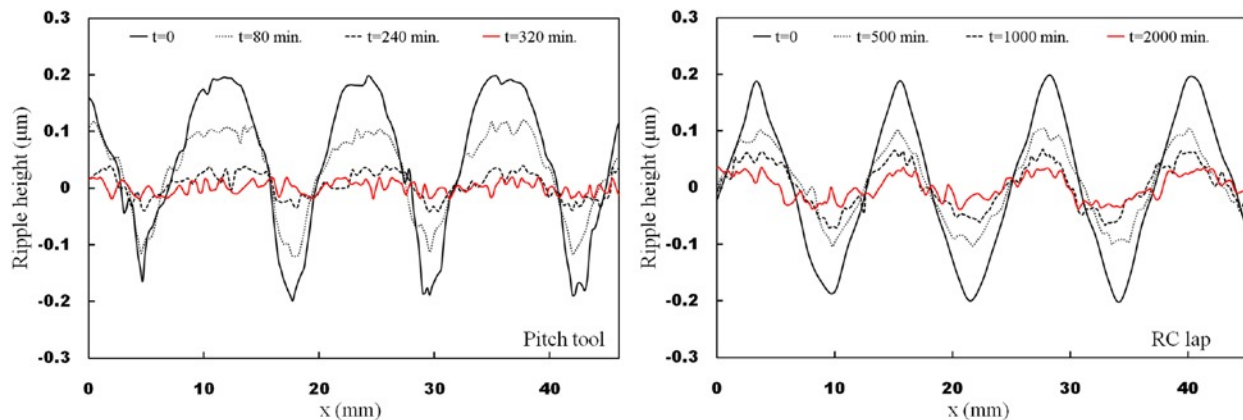

Figure 2. Surface profiles showing the reduction in ripples due to natural smoothing for pitch tools and for rigid conformal (RC) tools.[5]
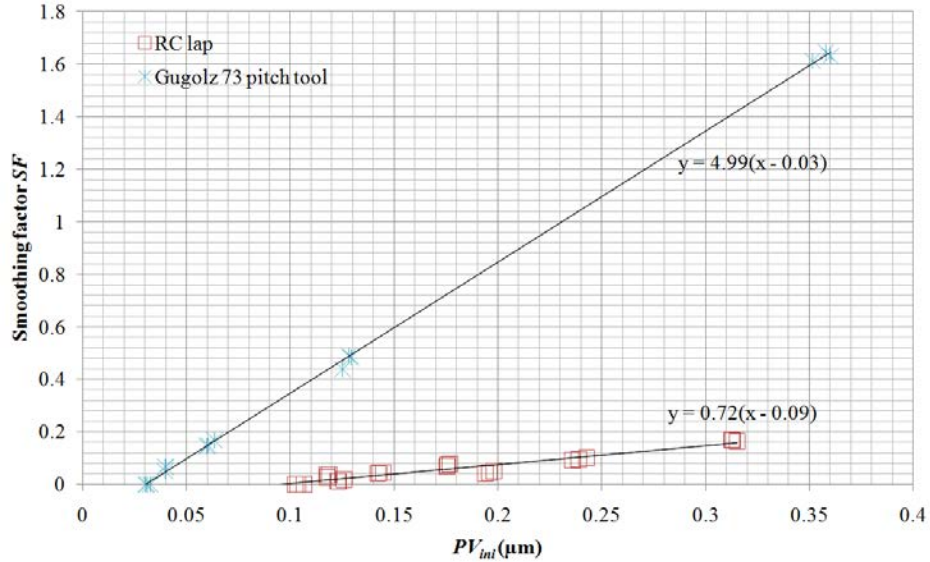
Figure 3. Measured smoothing factor as a function of the initial PV irregularity for classical tool with Gugolz 73 pitch and for the RC lap with LP66 polishing pads.[5] Note that this work calculates the smoothing factor with ε defined as PV irregularity for sinusoidal ripples a fixed frequency.

The results of the controlled smoothing experiments are striking. For both types of tools, the smoothing factor has a linear variation with ε_0 the initial surface irregularity and both go to zero at a threshold value, below which no smoothing occurs. As shown in Figure 3, the value of the slope and threshold vary for different polishing processes. Fitting the data to two parameters, the smoothing factor can be approximated as

$$SF = k \cdot \left(\varepsilon_{ini} - \varepsilon_0 \right)$$

Eq. 2

This work has been extended to high spatial frequencies, evaluating the evolution of the power spectral density (PSD) for various lap types. Figure 4. shows an evolution of the high frequency PSD as a surface is polished using conventional pitch #64 with Opaline polishing compound.[6]
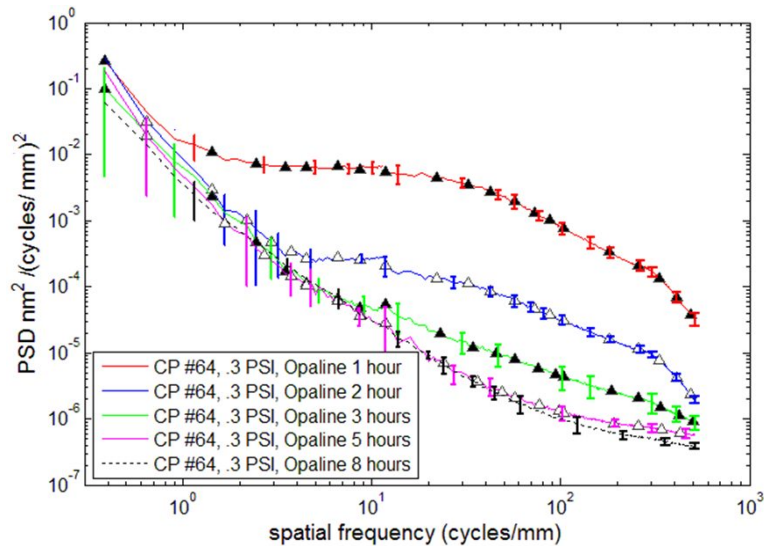

Figure 4. The surface high frequency irregularity relies entirely on natural smoothing. This figure shows the evolution of the high frequency PSD as the surface is polished using Opaline polishing compound with a lap made of #64 pitch.[6]

The smoothing factor as defined above works well for the case where well-defined sinusoidal irregularities are improved by natural smoothing under controlled tests. This allows the smoothing effect of polishing tools to be engineered and measured explicitly.[7] But surfaces being fabricated are much more complex. Rather than a single frequency, a full spectrum of irregularities is always present. In addition to the natural smoothing that improves the surface, some artifacts are frequently created by imperfect tool behavior. Also the measurements are never perfect, and the ability to accurately assess smoothing relies on subtracting data sets, which inherently amplifies any noise. These effects are accommodated for real polishing runs using a correlation based smoothing model where the smoothing factor includes only changes in the surface that are correlated with the initial surface irregularities.[8] The smoothing factor applies for this case, but the definition of ε_{ini} and ε' are changed to the root mean squared irregularity with period smaller than the tool.

The correlated smoothing was quantified for two different types of tools running on 8.4-m mirrors. The same linear behavior of the smoothing factor as described by Eq. 2 was maintained for different size and type of laps, faced with pitch or polishing pads. Figure 5 shows the 80-cm diameter (contact area) stressed lap shown polishing the LSST tertiary mirror and a 25-cm Rigid Conformal (RC) tool polishing one of the GMT primary mirror segments.

Figure 5. Large mirrors are polished with a variety of tools including the stressed lap shown polishing the LSST tertiary mirror on the left and a rigid conformal tool working one of the GMT segments shown on the right.

An example of the smoothing performance of the laps is provided for the case of the LSST tertiary mirror, polished by both 80-cm stressed lap and 35-cm RC tools, both faced with LP66 polishing pads. The smoothing factor follows the same linear trend, and is shown fit to this data in Figure 6.
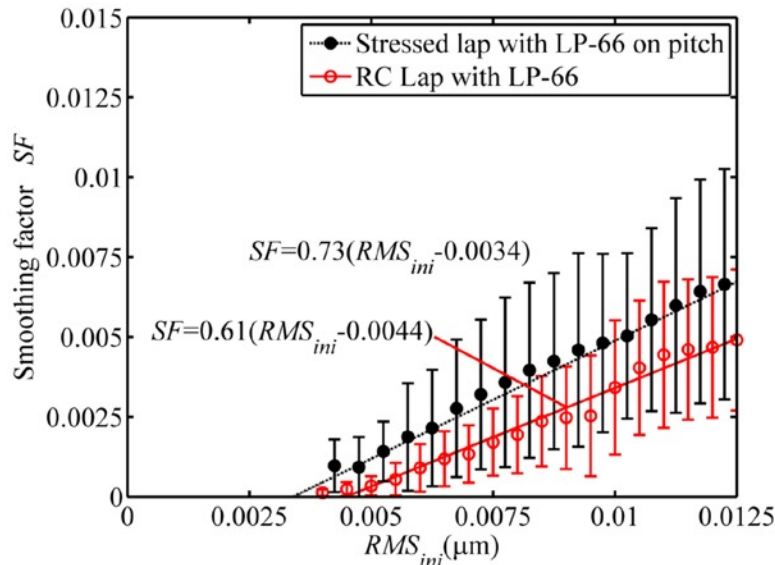

Figure 6. Smoothing Factor from polishing runs on the LSST tertiary mirror for two types of laps.[8]

The smoothing factor provides useful information for a single polishing run. But this provides only a snapshot of the surface improvement for this particular state. It is also useful to integrate the smoothing to evaluate the full evolution of the surface due to smoothing. It has been shown that the surface irregularity falls off as an exponential decay.[9] We provide an explicit derivation of this by combining Eq 1 and Eq. 2. and rewriting as a differential equation in Eq. 3 where ε represents the RMS surface irregularity as a continuous function of DC removal z and ε_0 is the threshold RMS irregularity, below which there appears no smoothing.

$$\frac{\varepsilon_{ini} - \varepsilon'}{\Delta z} = SF = k \cdot \left(\varepsilon_{ini} - \varepsilon_0 \right) \text{ for a single polishing run}$$

$$\frac{d\varepsilon(z)}{dz} = \frac{d\left(\varepsilon(z) - \varepsilon_0 \right)}{dz} = -k \cdot \left(\varepsilon(z) - \varepsilon_0 \right) \qquad \textbf{Eq. 3}$$

The solution to Eq. 3 is simply an exponential, shown in Eq. 4. We define constant $z_0 = \dfrac{1}{k}$ and substitute

$$\varepsilon(z) = \varepsilon_0 + \left(\varepsilon_{ini} - \varepsilon_0 \right) e^{-z/z_0} \qquad \textbf{Eq. 4}$$

Applying Eq. 4 to the data shown in Figure 6 is straightforward. Using data from the stressed lap, k = 0.73 and ε_0 is 0.0034 µm. So z_0 is 1.37 µm, which means that each time 1.37 µm is polished off of the surface, the irregularity becomes 63% closer to the asymptotic value of ε_0.
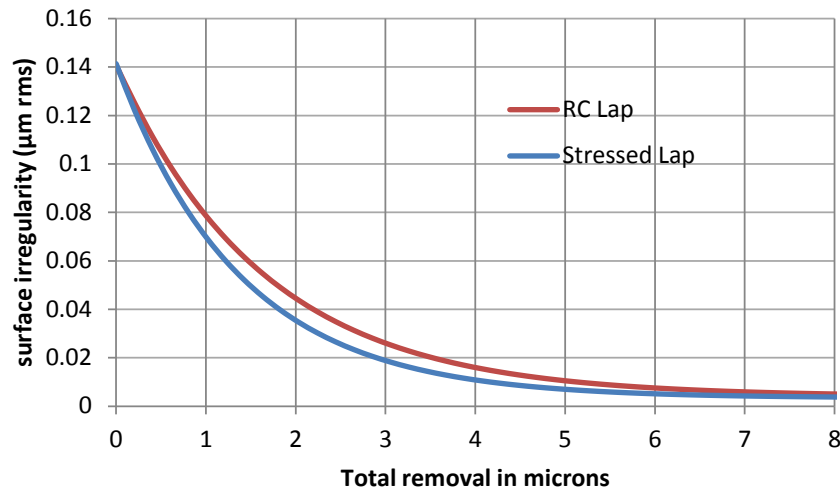

Figure 7. Exponential decay of the surface irregularity for a surface that starts with 0.14 µm rms, for polishing with the RC lap and the stressed lap with smoothing factors shown in Figure 6.

The optimization of the smoothing effect involves several parameters. The lap type, polishing compound, and stroke can be chosen to provide the maximum smoothing effect.[7,10] For a given process, the smoothing simply requires ample material removal. The total removal can be written using Preston's equation as a function of the polishing time t as

$$z(t) = \frac{A_{lap}}{A_{mirror}} K \cdot P \cdot V \cdot t \qquad \textbf{Eq. 5}$$

where

A_{lap} and A_{mirror} are the respective areas of the polishing lap and the mirror being worked
P is the lap pressure
V is the mean velocity of the lap over the mirror surface
K is Preston's constant, ~12 µm/hr / psi / (m/s) for cerium oxide polishing of borosilicate glass

For polishing of glass mirrors, we take the example of circular tools with the following:
- an orbital stroke with offset a of ¼ of the tool diameter D_{LAP},
- polishing pressure P, typically 0.3 psi
- stroking speed, Ω typically 30 – 90 rpm
- Instantaneous lap velocity $V = 2\pi a \Omega/60$ (a in meters, Ω in RPM, V in m/s)

The removal as a function of time is simply

$$z(t) = \frac{D_{lap}^2}{D_{mirror}^2} KP(2\pi \frac{D_{lap}}{4})\frac{\Omega}{60}t \cong 0.026\frac{D_{lap}^3}{D_{mirror}^2} KP\Omega t \qquad \textbf{Eq. 6}$$

where

D_{lap} and D_{mirror} are the respective diameters of the polishing lap and the mirror in meters
t is the machine time in hours
$z(t)$ is the removal in microns

Since removal and time are proportional, we can simply evaluate the time constant for the exponential surface improvement as τ where

$$\tau = 38\frac{D_{mirror}^2}{D_{lap}^3 KP\Omega}z_0 \qquad \textbf{Eq. 7}$$

Figure 8 illustrates the case of a 1-m mirror polished with a 0.6-m lap at 10 rpm, we can expect a 1/e time constant for the smoothing of the surface irregularity of 6.7 hours. It will take 2.3 times this, or 15 machine hours to improve the surface irregularity above the threshold by a factor of 10.
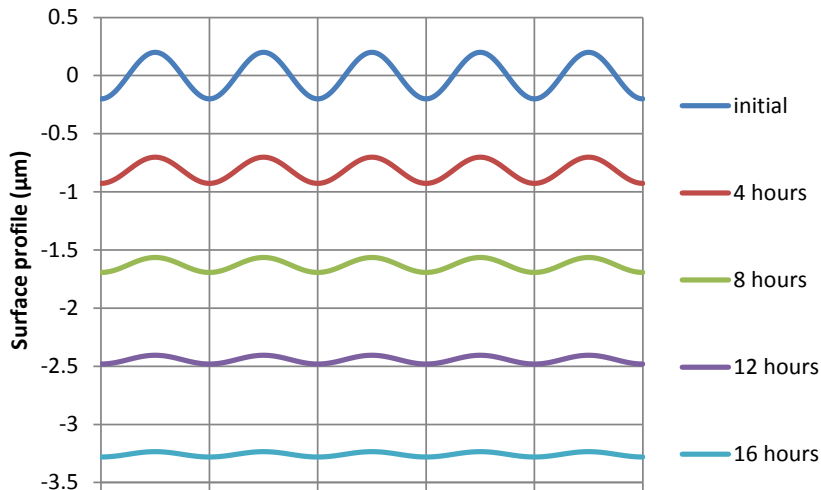

Figure 8. Evolution of a surface that starts with 0.14 µm rms, and is polished with a stressed lap with smoothing factor shown in Figure 6, with z_0 of 1.37 µm and ε_0 of 0.0034 µm.

3. DIRECTED FIGURING

Optical surfaces are finished using a combination of smoothing described above and directed figuring, in which the process is adjusted to achieve removal variations across the work piece. The most common method uses dwell time – the tool spends more time over regions that require more removal. The tool influence function is calibrated, and the dwell time is optimized for each position on the mirror.[11] This process is fundamentally different than natural smoothing because it relies on the accuracy of the surface measurements and on the ability of the polishing mechanism to provide accurate and stable removal. Directed removal is quite effective when the polishing machine spends more time on high regions and avoids low regions, as correctly provided by the measurements. However, directed figuring can degrade the surface if there are errors in the data (either magnitude of irregularity or the mapping) or if the removal is not predictable (either in the wear rate, profile, or position.)

The efficiency of the directed figuring can be quantified in a similar manner as the natural smoothing. However, we must accommodate two principal differences. The smoothing appears to be fairly constant for irregularities with different periods as long as they are small compared to the lap size. Larger periods are not affected by smoothing. The convergence of directed figuring is excellent for spatial periods that are large compared to the lap. The effect on smaller periods is nonlinear. The directed figuring may improve the frequency being addressed, but will create higher frequency errors that are referred to as "tool marks."

We perform direct evaluation for circular tools that are driven in a circular orbit. Such a tool creates removal according to the Tool Influence Function (TIF) shown in Figure 9. We evaluate the ability to correct a range of frequencies by direct simulation using a surface with 200 mm period, 0.4 µm PV, 0.14 µm rms sinusoidal ripples, as shown in Figure 10. Different sized tools are used for simulations that each target the sinusoidal error. The polishing time and the residual after correction are used to determine normalized performance parameters.
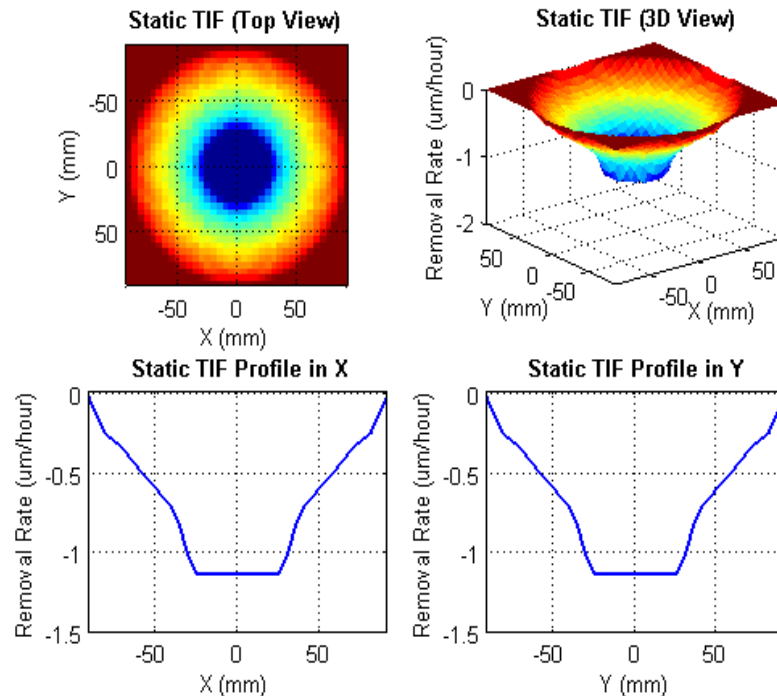

Figure 9. Example of a Tool Influence Function (TIF) for a 120 mm diameter tool stroked with an orbital radius of 30 mm.
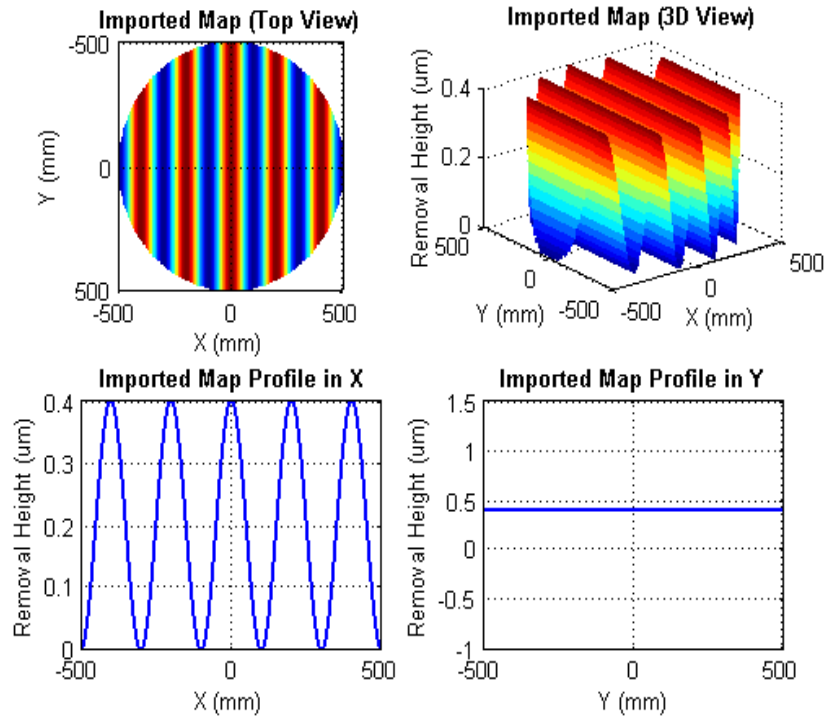
Figure 10. A 1-m surface with 0.14 µm rms ripples at 200 mm periods was used to determine performance of optimized polishing with different tool sizes.

The dwell time for each run was fully optimized to minimize the rms residual, after the run is finished. An example is shown in Figure 11, showing a simulation of a 120 mm tool, running with 30 mm orbital stroke radius at 100 rpm and 0.3 psi. The operation takes 14.6 hours to minimize the rms, leaving a residual of 0.008 µm rms.

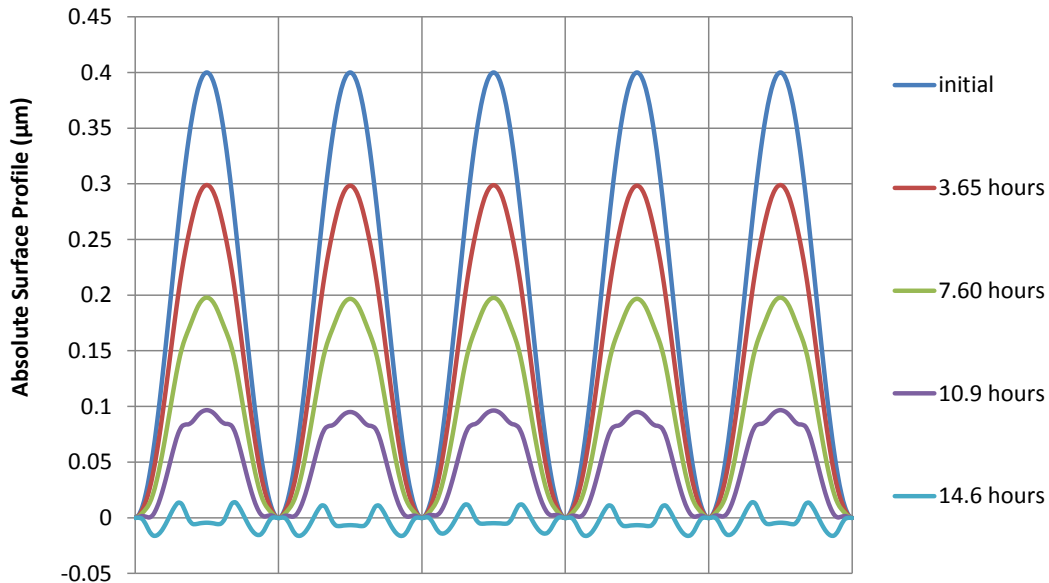**Figure 11.** Evolution of a surface that starts with 0.14 µm rms, and is polished with an optimal stroke with a 180 mm diameter TIF.
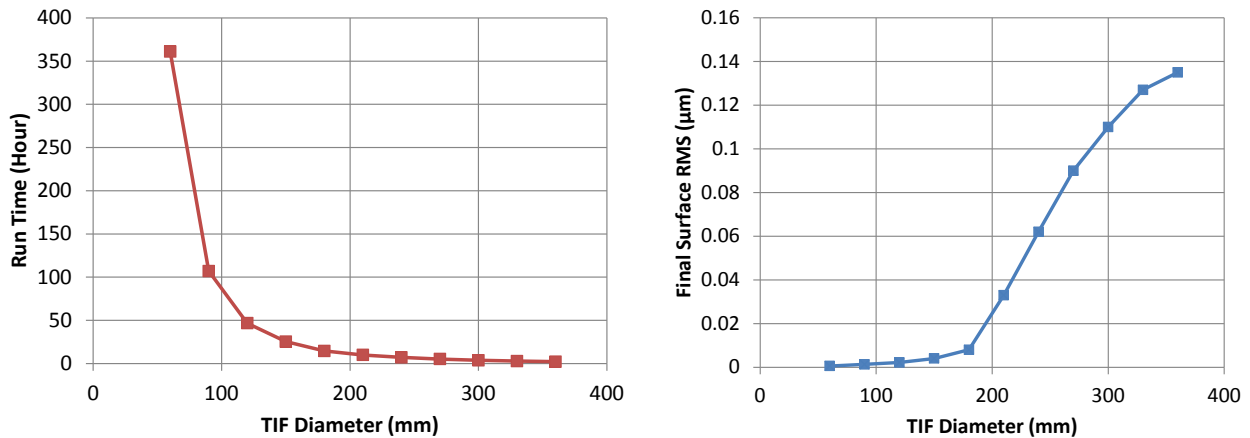
Figure 12. Optimization simulation runs were performed to correct sinusoidal irregularity with 0.4 µm PV (0.14 µm rms) and 200 mm period for a 1-m optic. The Tool Influence Function diameter was varied from one run to the next. The total polishing time and the residual after optimization are shown here.

These data are normalized into two functions:

- <u>Efficiency</u>, defined as the improvement in the surface per micron of mean removal, units are µm rms/µm.
- <u>Normalized Residual</u>, defined as the rms residual created per rms corrected, units are µm rms/µm rms

Both the efficiency and the normalized residual show a transition zone between tools being large compared to the period and tools that are small. Such data is well fit using a classic sigmoid or S-curve function, which is generally written using three parameters, A, $D_{\frac{1}{2}}$, and w.

$$S(D) = \frac{A}{1 + e^{-\frac{(D - D_{1/2})}{w}}}$$

Eq. 8

The data from Figure 12 is normalized and fit to the sigmoid function, as shown in Figure 13. The values from the fit are provided in Table 1. Note that these are normalized, so they can be easily scaled for any size tool or any removal rate.
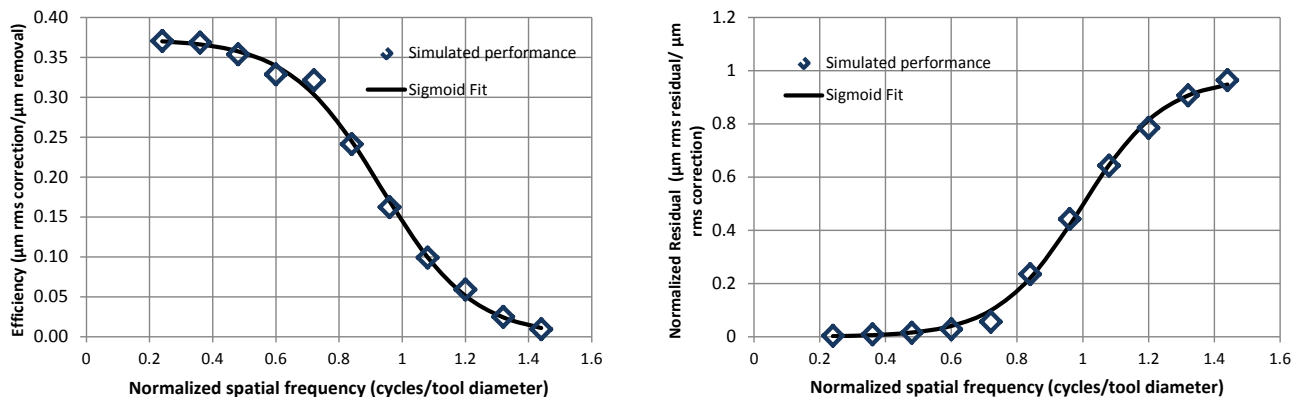

Figure 13. Normalized parameters taken from the simulations for orbital polishing of sinusoidal surface irregularity as a function of the spatial frequency. A 3-parameter sigmoid fit is used to describe the data.

Table 1. Sigmoid fit parameters from the data in Figure 13.

	Efficiency	*Normalized Residual*
A	0.37 µm rms/µm	0.98 µm rms/µm rms
D½	0.93 cycles/tool diameter	1.00 cycles/tool diameter
w	-0.145 cycles/tool diameter	0.126 cycles/tool diameter

4. PROCESS OPTIMIZATION

The parametric relations for smoothing and for directed removal allow quantitative predictions of performance without performing simulations. Such predictions lend themselves to parametric process optimization, where parameters that describe the manufacturing can be adjusted and optimize to produce higher performance surfaces or to increase efficiency. As an example for this paper, we choose to evaluate the polishing of a 1-m diameter surface. We evaluate the improvement of surface error with 200 mm period.

We already showed the surface improvement due to natural smoothing with a 600 mm lap. We compare this with the performance of a small tool using directed figuring. The orbital speed is 100 rpm, the pressure is 0.3 psi, and the Preston constant is 12 µm/(m/s)/psi/hr. Figure 14 clearly shows a few points:

- Smoothing is superior to directed figuring for the case where the smoothing lap is greater than several periods across and irregularities are large.

- Directed figuring with tools that are greater than 70% of the period shows good efficiency, but the residual created is too large. The data should be filtered before optimizatin to avoid such problems.

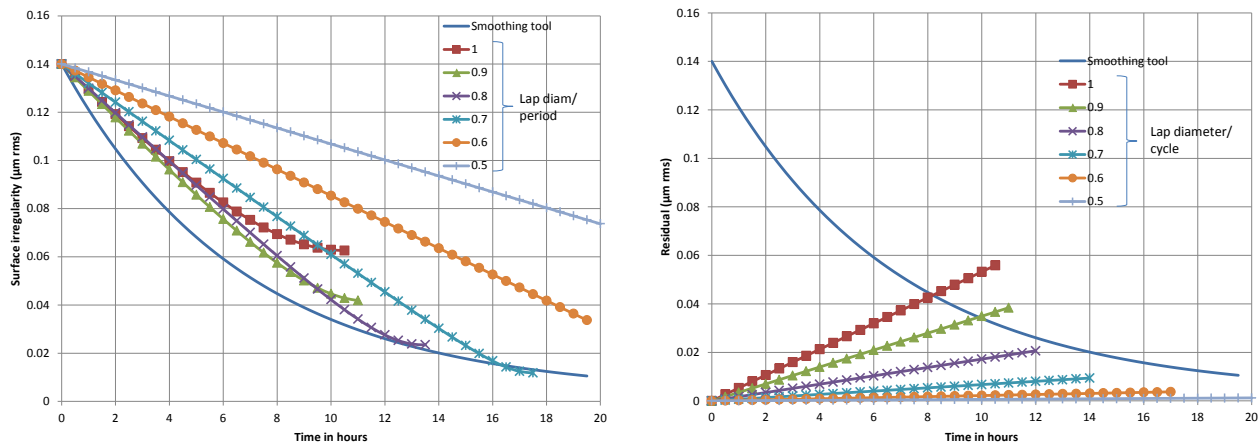- The tools smaller than 70% of the period create very little residual, but are extremely slow.

Figure 14. Surface evolution for directed figuring with laps that vary from 1 x the spatial period of the ripples to ½ times this period. As the sinusoidal irregularity improves for the case of directed figure, the smaller scale residual grows. As the smoothing tool operates, the residual amount of the original irregularity decreases exponentially.

It is instructive to evaluate the rate of change of the surface irregularity, which is readily provided using the parametric models. Figure 15 shows the rate of improvement due to natural smoothing and Figure 16 shows the rates for directed figuring (surface correction and creation of residual) as functions of the tool size.
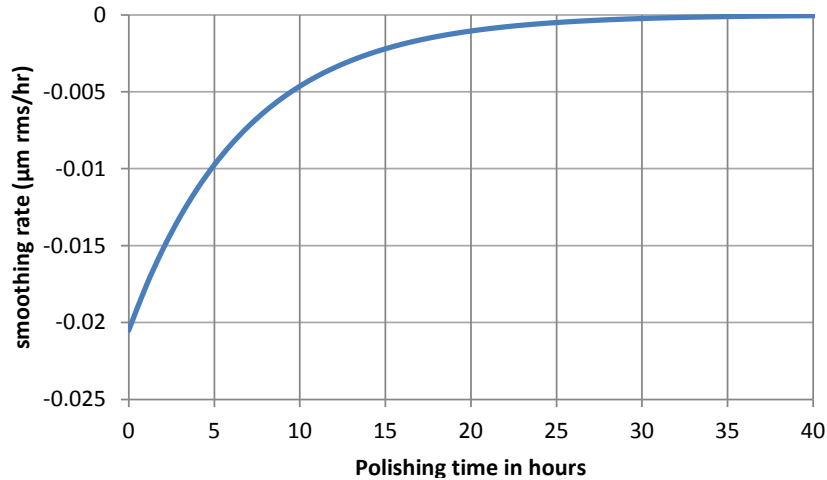
Figure 15. Rate of change for surface irregularity due to natural smoothing with a 60 cm lap.
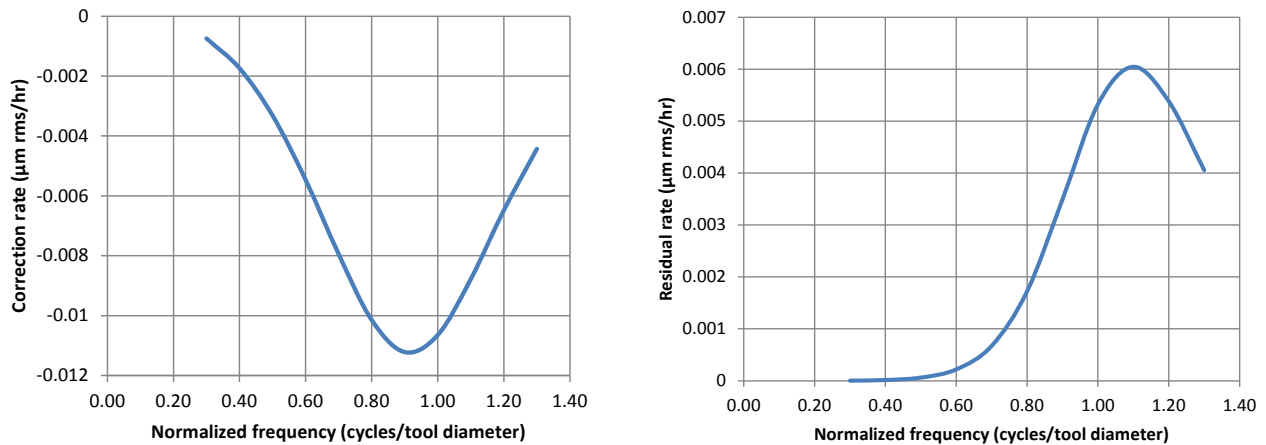

Figure 16. Rate of change for surfaces due to directed figuring with different size tools as described above.

Improved efficiency and final surface quality can be achieved using a combination of two tools:

1. Use a large smoothing tool first. Continue until the rate of improvement of the smoothing is less than that for directed figuring

2. Switch to small tool directed figuring. Evaluate time to complete and the residual tool marks created from this

If necessary, even smaller tools could be used to correct the tool marks or other errors introduced into the surface,[12] or specialized tools can be run on the edges.[13] We evaluate an optimized two-step process for various sizes of orbital tools, but the transition point for each is optimized to occur when the correction rate matches the smoothing rate. A set of cases with different tools is shown in Figures 17 and 18. These figures illustrate an important tradeoff between efficiency and final quality. Compare the performance of the tool that is 0.5 times the period with the largest one considered here, with diameter 0.8 times the period. The smaller tool performs better, achieving surface quality below 0.001 µm rms in 20 hours. But most surfaces do not require such quality. The larger tool can achieve 0.012 µm rms in only 11 hours. The smaller tool requires 16 hours to achieve the same results.
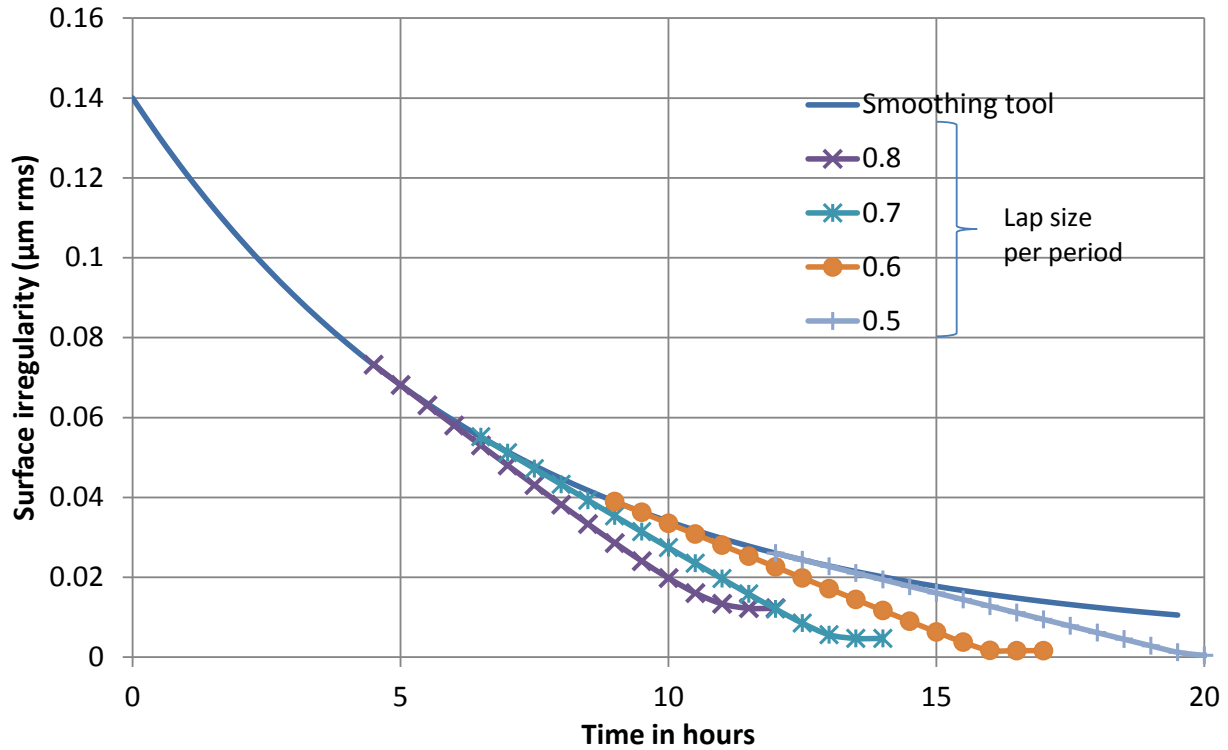
Figure 17. Evolution of the surface figure for an optimized combination of a 60 cm smoothing tool followed with small tool directed figuring. The transition point between the two operations is optimally chosen to occur when the directed removal rate just exceeds that of passive smoothing.
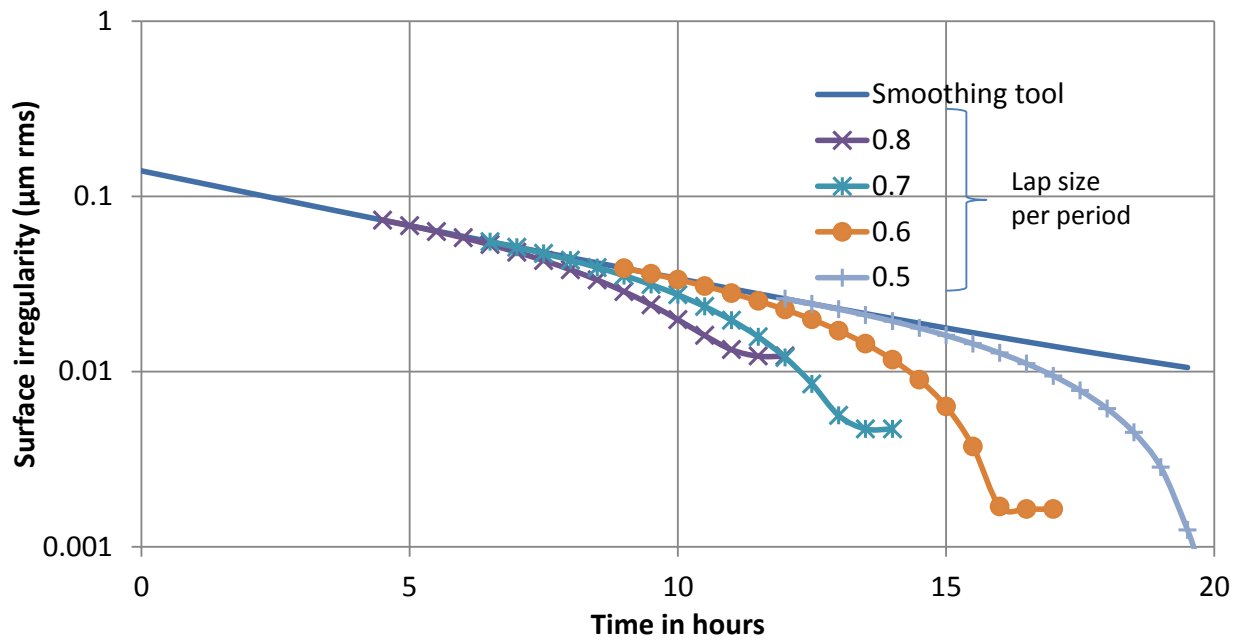

Figure 18. Same data as shown in Figure 17, shown here on a log scale.

5. CONCLUSION

We provide parametric relations that allow quantitative estimate of the performance of the polishing process in terms of the natural smoothing of features smaller than the lap and directed figuring for features larger than the lap. The initial evaluation of the simple case of a single sinusoidal surface error shows the value of these models. The parametric relations can be used to optimize the choice of the polishing tool for directed figuring to either achieve the fastest or the highest quality result. A more general solution can be built into the SAGUARO processing platform [14] that accommodates a complete power spectrum. Also, these models can be extended to loose abrasive grinding or shear mode grinding.[15]

We note that this analysis simplifies a complex interaction between the surface measurement uncertainty and the choice of parameters. For example, the choice of using the smallest tool allows correction with the least residual, but this is most sensitive to errors in the measurements that are used to optimize the polishing run and to instability or inaccuracy of the polishing tool. A variety of surface measurement techniques are used to provide a full range of spatial frequency information.[16] If the confidence in metrology and polishing controls could also be quantified, then this information could also be applied to optimize the full process.

REFERENCES

1) M. Tuell, J. H. Burge, and B. Anderson, "Aspheric optics: smoothing the ripples with semi-flexible tools." *Optical Engineering* **41**(7) pp. 1473-1474 (2002).

2) D. W. Kim and J. H. Burge, "Rigid conformal polishing tool using non-linear visco-elastic effect," Opt. Express **18**, 2242-2257 (2010).

3) H. M. Martin, R. G. Allen, J. H. Burge, B. Cuerden, D. W. Kim, J. S. Kingsley, K. Law, R. Lutz, P. A. Strittmatter, P. Su, M. T. Tuell, S. Warner, S. C. West, P. Zhou, "Production of 8.4 m segments for the Giant Magellan Telescope," Proc. SPIE **8450** (2012).

4) M. T. Tuell, H. M. Martin, J. H. Burge, D. A. Ketelsen, K. Law, W. J. Gressler, C. Zhao, "Fabrication of the LSST monolithic primary-tertiary mirror," Proc. SPIE **8450** (2012).

5) D. W. Kim, W. H. Park, H. K. An, and J. H. Burge, "Parametric smoothing model for visco-elastic polishing tools," Opt. Express **18**, 22515-22526 (2010).

6) J. G. Del Hoyo, DW. Kim, J. H. Burge, "Super-smooth optical fabrication controlling high-spatial frequency surface irregularity," Proc. SPIE **8838,** 88380T (2013).

7) X. Nie, S. Li, F. Shi, and H. Hu, "Generalized numerical pressure distribution model for smoothing polishing of irregular midspatial frequency errors," Appl. Opt. 53, 1020-1027 (2014).

8) Y. Shu, D. Kim, H. Martin, and J. H. Burge, "Correlation-based smoothing model for optical polishing," Opt. Express **21**, 28771-28782 (2013).

9) Y. Shu, X. Nie, F. Shi, and S. Li, "Smoothing evolution model for computer controlled optical surfacing," J. Opt. Technol. 81 (3), (2014).

10) Y. Shu, X. Nie, F. Shi, S. Li, "Compare study between smoothing efficiencies of epicyclic motion and orbital motion," *Optik* (2014)

11) D. W. Kim, H. M. Martin, J. H. Burge, "Calibration and optimization of computer-controlled optical surfacing for large optics," Proc. SPIE **8126** (2011).

12) D. W. Kim, S. W. Kim, and J. H. Burge, "Non-sequential optimization technique for a computer controlled optical surfacing process using multiple tool influence functions," Opt. Express **17**, 21850-21866 (2009

13) D. W. Kim, W. H. Park, S.-W. Kim, and J. H. Burge, "Parametric modeling of edge effects for polishing tool influence functions," Opt. Express **17**, 5656-5665 (2009).

14) D. W. Kim, B. J. Lewis, J. H. Burge, "Open-source data analysis and visualization software platform: SAGUARO," Proc. SPIE **8126** (2011).

15) J. B. Johnson, D. W. Kim, R. E. Parks, and J. H. Burge, "New approach for pre-polish grinding with low subsurface damage," Proc. SPIE **8126** (2011).

16) M. J. Valente, B. J. Lewis, N. Melena, M. A. Smith, J. H. Burge, "Advanced surface metrology for meter-class optics," Proc. SPIE **8838**, 88380F (2013).